OPEN ACCESS Freely available online

AFM Applied Functional Materials

ISSN 2737-5323
Volume 2, Issue 2
https://www.iikii.com.sg/journal/AFM
Applied Functional Materials

Article

Photovoltaic Performance of $CH_3NH_3PbI_2Cl$ Perovskite Solar Cell

Yi-Tzu Tseng, Yu-Ting Tseng and Chia-Ching Wu *

Department of Applied Science, National Taitung University, Taitung, Taiwan 95092, R.O.C.
* Correspondence: ccwu@nttu.edu.com; Tel.: +886-89-318855

Received: May 19, 2022; **Accepted:** Jun 19, 2022; **Published:** Jun 30, 2022

Abstract: Perovskite solar cells have attracted extensive research attention recently as they are promising high-performance solar cells with long-time stability at a low cost. In this study, we demonstrated a one-step solution approach to prepare the $CH_3NH_3PbICl_2$ perovskite layer by adding lead chloride ($PbCl_2$) to the standard methylamine iodide (MAI) precursor solution and annealing process of the perovskite layer at different temperature. Finally, the Ag/Spiro-OMeTAD/$CH_3NH_3PbI_2Cl$ /mp-TiO_2/c-TiO_2/FTO/Glass perovskite solar cell was successfully fabricated by using solution processing.

Keywords: $CH_3NH_3PbI_2Cl$, TiO_2, Spiro-MeOTAD, Perovskite solar cell

1. Introduction

Global energy requirement has been continually increasing with industrial development and population growth in recent years. To date, over 85% of energy attrition is generated from fossil fuels, which causes environmental pollution and climate change. In this context, the solar cell is one of the most promising technologies that directly convert sunlight into electricity. Solar energy possesses cost-effective, reliable, and safe attributes [1,2].

The first solar cell was fabricated by using the silicon p–n junction. The silicon solar cells are currently leading the commercial photovoltaics markets with a share of 85%. The best power conversion efficiency (PCE) of the silicon solar cell is about 28% (NREL: Best research cell efficiency). In recent years, perovskite solar cells (PSCs) have received extensive attention owing to their potential for achieving lightweight, cheap, and facile fabricated solar cells [3]. The perovskite solar cell is a semiconductor with a special crystal structure that makes them well suited for solar cell technology and can be manufactured at room temperature with much less energy and more sustainability to produce than the silicon solar cell.

The organic-inorganic hybrid metal halide perovskite has a crystal structure with the general formula ABX_3 composed of small organic cations (A^+), metal cations (B^+), and halide anions (X^-). Methylammonium lead ($CH_3NH_3PbX_3$, X = I, Br, or Cl) halide perovskites represent a novel class of absorbers for solar conversion applications [4]. Various perovskite materials (e.g., $CH_3NH_3PbI_3$, $CH_3NH_3PbI_{3-x}Cl_x$, and $CH_3NH_3PbBr_3$) and device composition (e.g., mesoporous and planar structures) have been investigated with promising results by using solution processing, thermal evaporation, or sputtering method [5–7]. The $CH_3NH_3PbBr_3$perovskite solar cells have attracted less attention than the iodide homologous. The relatively wide band gap of 2.3 eV limits the usable spectral range for single junction solar cells [8]. Most impressive, the $CH_3NH_3PbI_{3-x}Cl_x$ cells exhibit high V_{oc} values and reach qV_{oc}/E_{Gap} values of up to 0.71 and a remarkably high figure for a new type of cell [9]. In contrast to the success of $CH_3NH_3PbI_{3-x}Cl_x$ for planar devices, the solution process of $CH_3NH_3PbI_3$ has mainly been used in mesoporous cell structures [10].

The improvement of the PCE of PSCs is dependent on how to control the shape, interface defects, and passivation of perovskite thin films [11]. In this study, methylamine iodide (MAI) and lead chloride ($PbCl_2$) mixed with dimethylformamide (DMF) were used as the perovskite solutions for the fabrication of the $CH_3NH_3PbI_2Cl$ perovskite layer in the one-step spin-coating method. The different annealing temperatures were used to understand the effect on the perovskite layer. Finally, the Ag/Spiro-OMeTAD/ $CH_3NH_3PbI_2Cl$ /mp-TiO_2/c-TiO_2/FTO/Glass structure was fabricated as the perovskite solar cell.

2. Materials and Methods

2.1. Materials

All chemicals have been used without further purification. CH_3NH_3I (MAI, Sigma-Aldrich, 99.5%), Lead(II) chloride ($PbCl_2$, Sigma-Aldrich, 99.99%), Titanium isopropoxide (TTIP, Sigma-Aldrich, 97%), Titanium(IV) oxide (TiO_2, Sigma-Aldrich, 99.5%), Spiro-OMeTAD (Lumtec), Li-TFSI (Sigma-Aldrich), tert-butylpyridine (tBP, Sigma-Aldrich, 98%), chlorobenzene (Sigma-Aldrich,

99.9%), Dimethylformamide (DMF, Sigma-Aldrich) and silver target (Ag, Parekh Industries, 99.9%) were used for the perovskite solar cell device fabrication.

2.2. Fabrication of Solar Cell

Firstly, patterned FTO glass substrates were etched by using Zn powder and HCl. Then, the FTO substrates were ultrasonically cleaned with Hellmanex (c) III, deionized water, acetone, and isopropanol sequence. Afterward, they were dried with high-pure N_2 gas. Finally, the substrates were treated with UV-O_3 for 15 min. The surface SEM image of the FTO is shown in Fig. 1. The compact TiO_2 (c-TiO_2) and mesoporous TiO_2 (mp-TiO_2) as the electron-transport layer (ETL) deposited on the FTO substrate. The c-TiO_2 was prepared by the TTIP and diluted in ethanol as a precursor. The TTIP precursor was coated by spin coating method with a speed of 4000 rpm for 30 s and then dried at 150 °C for 1 h. Subsequently, ethanol dispersed mp-TiO_2 nanoparticles were spin-coated on the c-TiO_2 and dried at 600 °C for 1 h. The $CH_3NH_3PbI_2Cl$ perovskite solution, the MAI, and $PbCl_2$ were dissolved in pure DMF solvent and prepared in a glove box. The $CH_3NH_3PbI_2Cl$ solution was stirred for 2 h and filtered before use. For the solar cell device fabrication, the $CH_3NH_3PbI_2Cl$ perovskite solution was spin-coated on the c-TiO_2/FTO/Glass substrate at 2000 rpm for 30 s, and the substrate was annealed at 110 °C for 10 min. When the $CH_3NH_3PbI_2Cl$ /c-TiO_2/FTO/Glass substrate cooled down to room temperature, the spiro-OMeTAD solution as the hole-transport layer (HTL) was spin-coated on the $CH_3NH_3PbI_2Cl$ perovskite layer at 4000 rpm for 60 s. The samples were kept in a drier bin overnight. The spiro-OMeTAD solution was composed of spiro-OMeTAD, tBP, and Li-TFSI solution in chlorobenzene. Finally, 100 nm-thick silver (Ag) electrodes were deposited in a sputtering system. The effective active area of the solar cell device was 0.04 cm^2.

2.3. Measurement Equipment

The high-resolution scanning electron microscopy (HRSEM, SU8000, Hitachi Company) at 20 kV was used to observe the materials and devices' structure. The crystallography of the materials was measured through X-ray diffraction (XRD, D8 Discover, Bruker Company) with CuKα radiation (2θ = 20−60°). The absorption of the materials was measured by using an ultraviolet-visible (UV–vis) spectrophotometer (Analytik Jena). The current-voltage (I-V) curve of perovskite solar cells was measured by using Keithley 2450 source measuring unit under solar-simulated light (Class AAA Solar Simulators). The 100 mW/cm^2 (AM 1.5G) sunlight was calibrated with a standard Si-based solar cell.

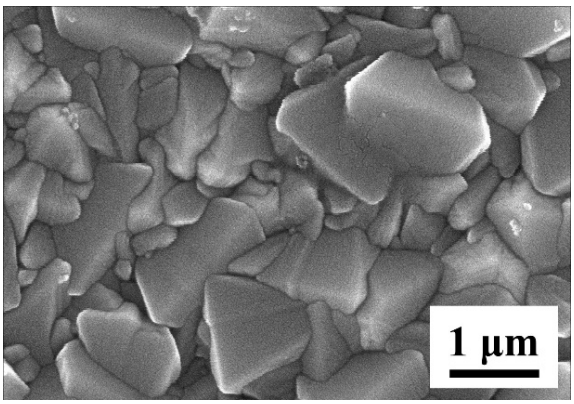

Fig. 1. SEM image of the FTO/Glass substrate.

3. Results and Discussion

To investigate the morphology and thickness of the c-TiO_2 layer, scanning electron microscope (SEM) measurements were performed. Figure 2 shows that the c-TiO_2 layer deposited on the FTO substrate has a mirror-like smooth surface morphology and the thickness of the c-TiO_2 layer of about 20 nm. Because the mp-TiO_2layer has a larger grain size than the c-TiO_2 layer, a less dense film is obtained. Therefore, the c-TiO_2 layer efficiently reduces the carrier recombination induced by the direct contact between the $CH_3NH_3PbI_2Cl$ perovskite layer and the FTO substrate. The mp-TiO_2 nanoparticles are dispersed in different ethanol contents as shown in SEM images (Fig. 2). The ratio of the TiO_2 nanoparticles and ethanol is equal to 1:2, and the thickness of the mp-TiO_2 layer is 432 nm (Fig.2(a)). When the ratio of the TiO_2 nanoparticles and ethanol is equal to 1:4, the thickness of the mp-TiO_2 layer is 257 nm (Fig. 2(b)). The thickness of the mp-TiO_2 layer decreases as the ethanol content increases. In Fig. 2(c), it is

found that the mp-TiO_2 layer has a large grain size than the c-TiO_2 layer, and the nanopores exist on the surface of the c-TiO_2 layer. In the mp-TiO_2/c-TiO_2/FTO/Glass structure, the pores act as nucleating sites for the $CH_3NH_3PbI_2Cl$ grain growth.

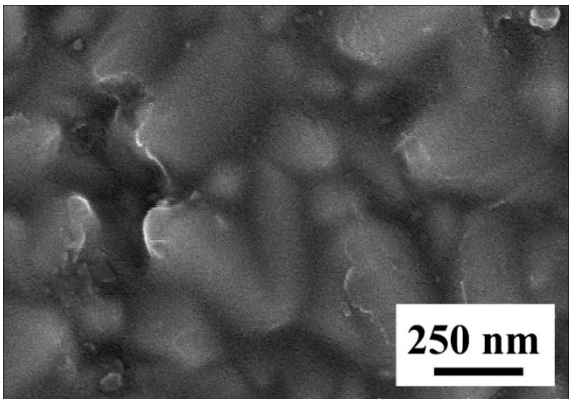

Fig. 2. SEM image of the compact TiO_2 deposited on FTO/glass substrate.

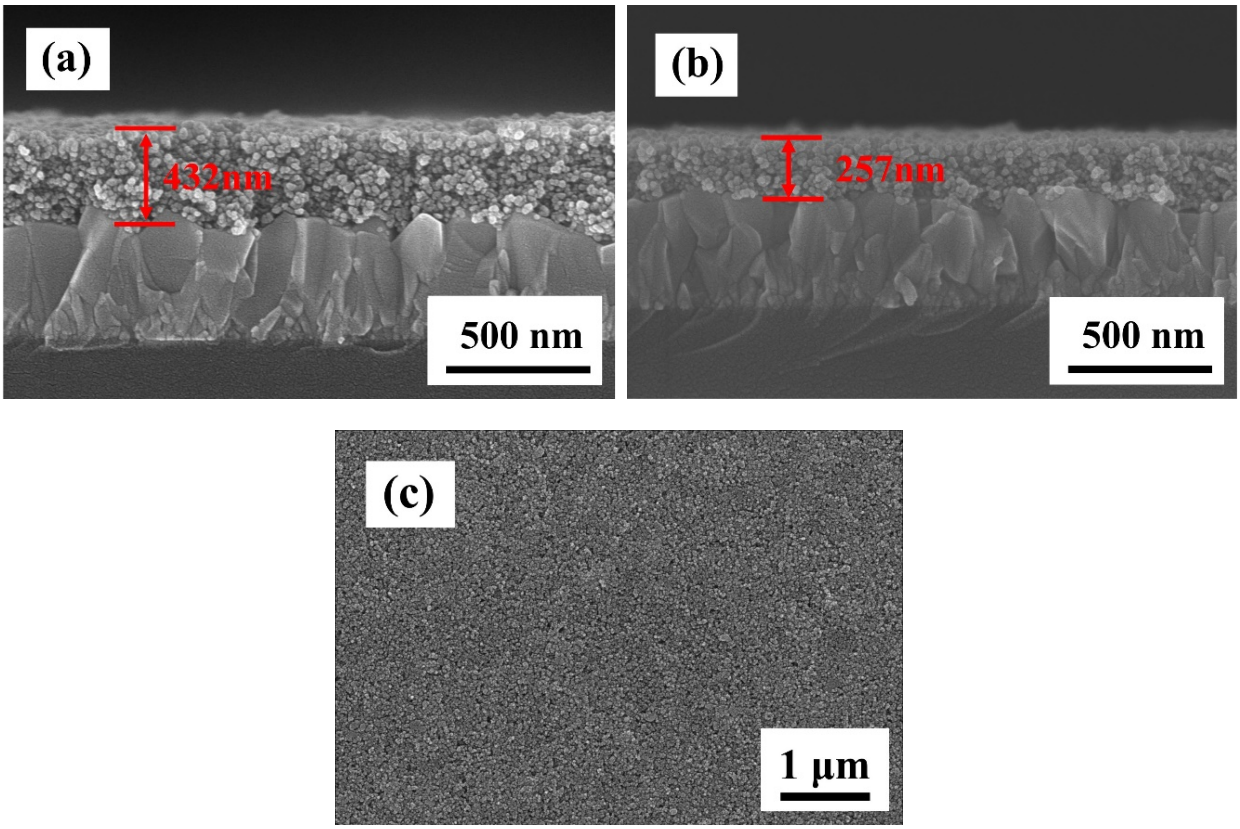

Fig. 3. Cross-section SEM image of mesoporous TiO_2 layer as the ratio of the TiO_2 nanoparticles and ethanol equal to (a)1:2 and (b)1:4. (c) The surface SEM image of the mesoporous TiO_2 layer.

Figure 4 shows the XRD pattern of the mp-TiO_2 layer. At the annealing temperature of 600 °C, the sharp peaks in the diffraction pattern are shown, which indicates that the high crystallinity of TiO_2 powder is obtained, and the diffraction peaks have good consistency with anatase TiO_2 and rutile TiO_2 (JCPDS 21-1272 and JCPDS 75-1537). No second phases or unknown phases exist in Fig. 4. This result demonstrated that the mp-TiO_2 is appropriate for application on ETL.

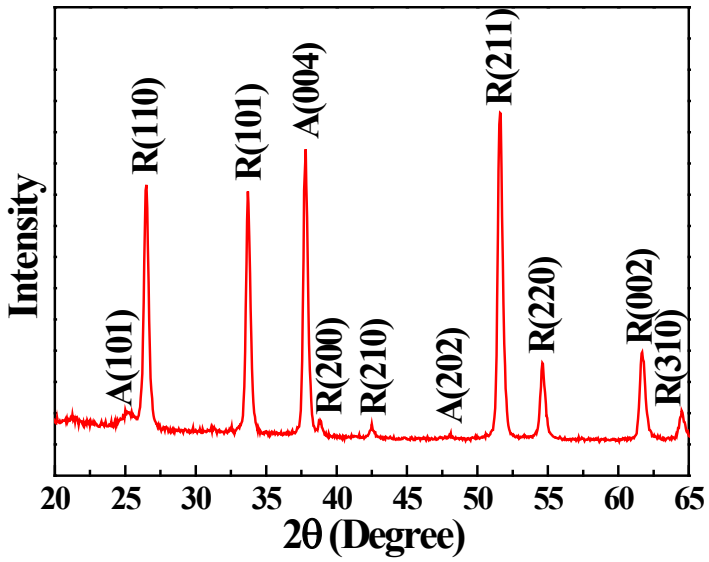

Fig. 4. XRD pattern of mesoporous TiO_2.

Figure 5 shows the SEM image of the surface of the $CH_3NH_3PbI_2Cl$ perovskite layer. At the annealing temperature of 80 °C, the large elongated crystal is formed with a significant portion of the FTO substrate that is exposed without $CH_3NH_3PbI_2Cl$ perovskite material coverage. When annealed at 110 °C, the elongated large crystal disappears, and the substrate is coated with relatively small crystals that are interconnected with a high surface coverage. The perovskite film is full of compact nanocrystals without pinholes, which makes the film smoother than sequentially deposited ones as shown in Fig. 5(b). The difference in the surface coverage of perovskite films affects the device characteristics.

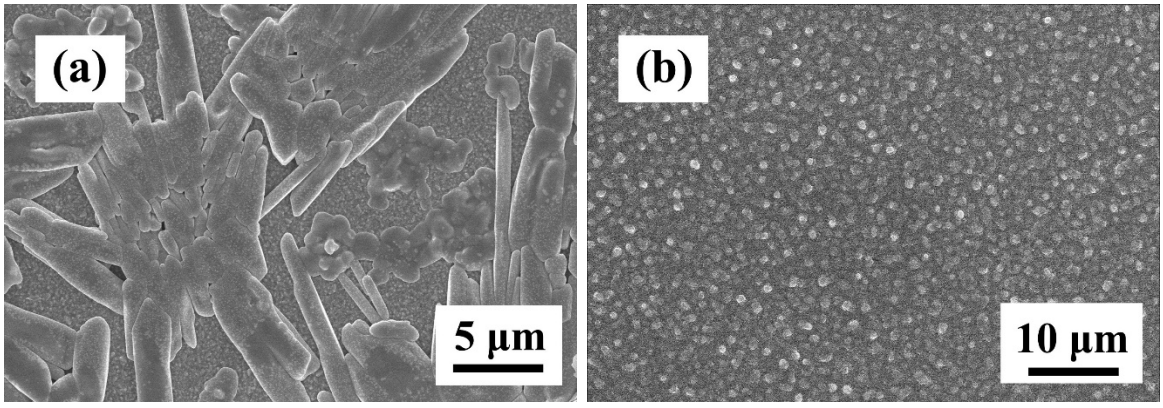

Fig. 5. SEM image of the surface of the $CH_3NH_3PbI_2Cl$ perovskite layer as the annealing temperature at (a) 80 oC and (b) 110 oC.

The X-ray diffraction (XRD) patterns of the CH3NH3PbI2Cl deposited on the FTO substrate as shown in Fig. 6. The diffraction peaks of the CH3NH3PbI2Cl perovskite material at 23.1°, 28.3°, 35.2°, 40.4°,43.1°, 48.2°, 53.9°, and 55.1° are apart from the three peaks from the FTO substrate (marked as o) [12,13]. No PbCl2 phases or unknown phases exist in Fig. 6. Figure 7 shows the UV-vis absorption spectra of the CH3NH3PbI2Cl perovskite layer at the annealing temperature of 110 °C. When the UV-vis light of different wavelengths irradiates the sample continuously, the absorption intensity corresponding to the wavelength is obtained. Figure 7 shows that the CH3NH3PbI2Cl perovskite layer has a strong excitonic absorption edge at 800 nm.

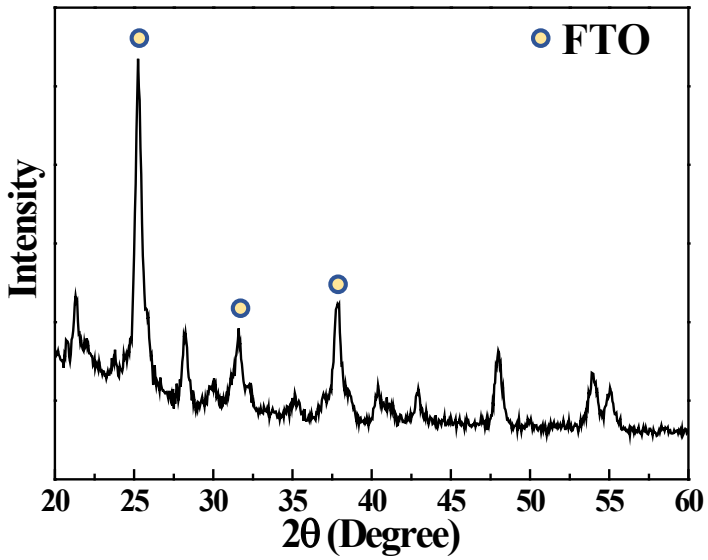

Fig. 6. XRD pattern of $CH_3NH_3PbI_2Cl$ perovskite layer at the annealing temperature of 110 °C.

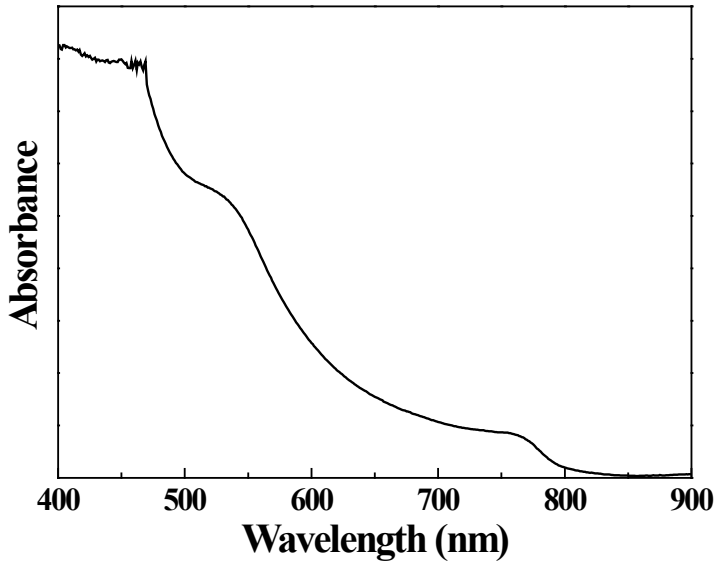

Fig. 7. UV-vis absorption spectra of $CH_3NH_3PbI_2Cl$ perovskite layer at the annealing temperature of 110 °C.

The overall power conversion efficiency (η) of the solar cell is calculated from the short-circuit photocurrent density (J_{sc}), open-circuit photovoltage (V_{oc}), fill factor (F.F.) of the cell, and the incident light intensity (P_{in} = 100 mW/cm^2). Therefore, the more square-like current density-voltage (J-V) curve of the $CH_3NH_3PbI_2Cl$ perovskite solar cell is essential for achieving the maximum value of F.F. (Fig. 8). η and F.F. values are calculated by using the following equation.

$$\eta = \frac{P_{max}}{E} = \frac{J_{sc} \times V_{oc} \times F.F.}{P_{in}} \quad (1)$$

$$F.F. = \frac{I_{max} \times V_{max}}{J_{sc} \times V_{oc}} \times 100\% \quad (2)$$

The perovskite solar cell demonstrates a J_{sc} of 0.03 mA/cm^2 , V_{oc} of 0.81 V, and F.F. of 0.641% to yield a η of 0.21%. Figure 9 shows the cross-section SEM image of the Spiro-OMeTAD/$CH_3NH_3PbI_2Cl$/mp-TiO_2/c-TiO_2/FTO/Glass structure. The thickness of the c-TiO_2, mp-TiO_2, $CH_3NH_3PbI_2Cl$, and piro-OMeTAD are 34, 245, 200, and 169 nm, respectively. In Fig. 9, it found that pores exist in the $CH_3NH_3PbI_2Cl$ perovskite layer, therefore, the η of the perovskite solar cell presents a lower value.

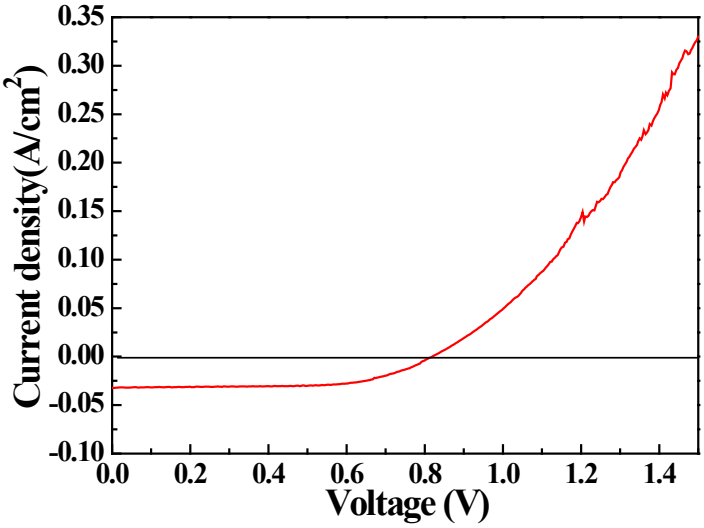

Fig. 8. I-V curves of the Spiro-OMeTAD/ $CH_3NH_3PbI_2Cl$ /mp-TiO_2/c-TiO_2/FTO/Glass perovskite solar cell.

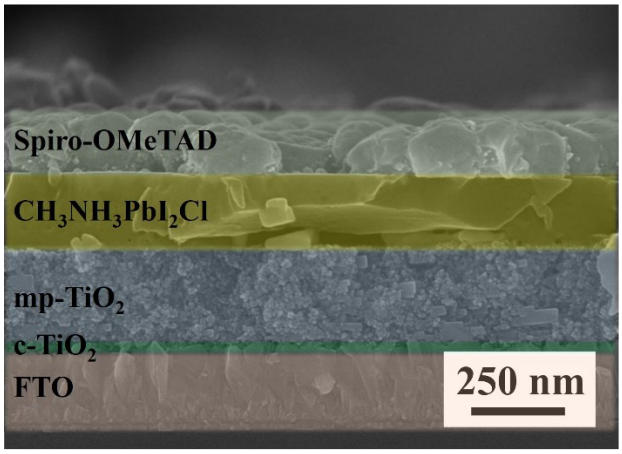

Fig. 9. The cross-section SEM image of the Spiro-OMeTAD/$CH_3NH_3PbI_2Cl$ /mp-TiO_2/c-TiO_2/FTO/Glass structure.

5. Conclusions

In summary, we prepare perovskite $CH_3NH_3PbI_2Cl$ on a mesoporous mp-TiO_2/c-TiO_2/FTO/Glass substrate with a one-step solution. From the SEM, XRD, and UV-vis analysis, it was found that the optimal annealing temperature of the $CH_3NH_3PbI_2Cl$ perovskite layer is set to 110 °C. The spiro-OMeTAD as the HTL deposition on the $CH_3NH_3PbI_2Cl$ perovskite layer and the $CH_3NH_3PbI_2Cl$ perovskite layer is kept in a desiccator overnight. Finally, the optimized perovskite solar cell was obtained with the Jsc of 0.03 mA/cm^2, Voc of 0.81 V, and F.F. of 0.641%, yielding a η value of 0.21%.

Author Contributions: The manuscript was written with the contributions of all authors. All authors have approved the final version of the manuscript. Yu-Ting Tseng performed the perovskite materials synthesis and analysis. Yi-Tzu Tseng performed the perovskite solar cell fabrication. Chia-Ching Wu (Corresponding Author) performed the design of this research, and analyzed the material and device, and wrote the article.

Funding: This research did not receive external funding.

Acknowledgments: The authors acknowledge the financial support of the Ministry of Science and Technology (MOST 110-2628-E-143-001, MOST 110-2731-M-006-001). The authors gratefully acknowledge the use of High-Resolution Scanning Electron Microscope (EM003600) equipment belonging to the Core Facility Center of National Cheng Kung University.

Conflicts of Interest: The authors declare no conflict of interest.

References

1. Shah, A.; Torres, P.; Tscharner, R.; Wyrsch N.; Keppner, H. Photovoltaic technology: the case for thin-film solar cells, *Science* **1999**, *285*, 692–698.
2. Zhang, H.; Ji, X.; Yao, H.; Fan, Q.; Yu, B.; Li, J. Review on efficiency improvement effort of perovskite solar cell, *Solar Energy*, **2022**, *233*, 421–434.
3. Ni, Z.; Jiao, H.; Fei, C.; Gu, H.; Xu, S.; Yu, Z.; Yang, G.; Deng, Y.; Jiang, Q.; Liu, Y.; Yan, Y.; Huang, J. Evolution of defects during the degradation of metal halide perovskite solar cells under reverse bias and illumination, J. Mater. Chem. A, *Nat Energy,* **2022**, *7*, 65–73.
4. Snaith, H. J. Perovskites: The Emergence of a New Era for Low-Cost, High-Efficiency Solar Cells. *J. Phys. Chem. Lett*. **2013**, 3623−3630.
5. Bi, D.; Yang, L.; Boschloo, G.; Hagfeldt, A.; Johansson, E. M. J. Effect of Different Hole Transport Materials on Recombination in CH3NH3PbI3 Perovskite-Sensitized Mesoscopic Solar Cells. *J. Phys. Chem. Lett.* **2013**, *4*, 1532−1536.
6. Chen, S.; Hou, Y.; Chen, H.; Richter, M.; Guo, F.; Kahmann, S.; Tang, X.; Stubhan, T.; Zhang, H.; Li, N. Nicola Gasparini, Cesar Omar Ramirez Quiroz,Laraib S. Khanzada,Gebhard J. Matt,Andres Osvet,Christoph J. Brabec, Exploring the Limiting Open-Circuit Voltage and the Voltage Loss Mechanism in Planar CH3NH3PbBr3 Perovskite Solar Cells, *Adv. Energy Mater*. **2016**, *6*, 1600132 (1–9).
7. Edri, E.; Kirmayer, S.; Mukhopadhyay, S.; Gartsman, K.; Hodes, G.; Cahen, D. Elucidating the charge carrier separation and working mechanism of CH3NH3PbI3−xClx perovskite solar cells, *Nature Communications*, **2014**, *5*, 3461(1–8).
8. Li, Z. ; Boix, P.P.; Xing, G.; Fu, K. ; Kulkarni, S.A.; Batabyal, S.K.; Xu, W.; Cao, A.; Sum, T.C.; Mathews, N.; Wong, L.H. Carbon nanotubes as an efficient hole collector for high voltage methylammonium lead bromide perovskite solar cells. *Nanoscale* **2016** , *8* , 6352 .
9. Lee, M. M.; Teuscher, J.; Miyasaka, T.; Murakami, T. N.; Snaith, H. J. Efficient hybrid solar cells based on meso-superstructured organometal halide perovskites. *Science* **2012**, *338*, 643–647.
10. Burschka, J.; Pellet, N.; Moon, S. J.; Humphry-Baker, R.; Gao, P.; Nazeeruddin, M. K.; Gratzel, M. Sequential Deposition as a Route to High-Performance Perovskite-Sensitized Solar Cells. *Nature* **2013**, *499*, 316−319
11. Wu, X.; Trinh, M.T.; Niesner, D., Zhu, H.; Norman, Z.; Owen, J.S.; Yaffe, O.; Kudisch, B.J.; Zhu, X.-Y. Trap States in Lead Iodide Perovskites. *J. Am. Chem. Soc.*, **2015**, *137*, 2089.
12. Zhao, Y.; Zhu, K. Charge Transport and Recombination in Perovskite (CH3NH3)PbI3 Sensitized TiO2 Solar Cells. *J. Phys. Chem. Lett.* **2013**, *4*, 2880−2884.
13. Zhao, Y.; Zhu, K. Optical Bleaching of Perovskite (CH3NH3)-PbI3 Through Room-Temperature Phase Transformation Induced by Ammonia. *Chem. Commun.* **2014**, *50*, 1605−1607.